A low-profile planar antenna for wireless sensor network with rotated A-shaped patch and defected ground plane

REZAUL AZIM[a,*], M. TARIQUL ISLAM[b], MD. MOTTAHIR ALAM[c], KHALID A. FAKEEH[d], MAHABOOB SHARIEF SHAIK[e]
[a]*Department of Physics, University of Chittagong, Chittagong 4331, Bangladesh*
[b]*Department of Electrical, Electronic & Systems Engineering, Faculty of Engineering & Built Environment, Universiti Kebangsaan Malaysia (UKM), 43600 Bangi, Malaysia*
[c]*Department of Electrical and Computer Engineering, King Abdulaziz University, Jeddah 21589, Saudi Arabia*
[d]*Department of Information Systems, King Abdulaziz University, Jeddah 21589, Saudi Arabia*
[e]*Department of Computer Science & Engineering, JJT University, Jhunjhunu, Rajasthan 333001, India*

A rotated A-shaped antenna working at around 2.45 GHz is presented for a wireless sensor network application. The studied antenna is comprised of an A-shaped patch and a small defected ground plane and is printed on both sides of the FR4 substrate material. One I-shaped parasitic slit is added to the tip of a rotated A-shaped patch to form a matching circuit that helps the studied antenna to excite at around 2.45 GHz. The experimental result shows that for $S_{11} \leq -10$dB, the presented antenna achieved an impedance band ranging from 2.3 to 2.57 (270 MHz) GHz. The studied antenna also attained appreciable gain, efficiency and exhibits a stable omnidirectional radiation pattern over the working band, which makes it suitable for sensor nodes.

(Received January 16, 2021; accepted October 7, 2021)

Keywords: A-shaped patch, Defected ground plane, Nodes, Parasitic slit, Planar antenna, Wireless sensor network

1. Introduction

Wireless sensor network (WSN) is the most standard service used in agricultural, commercial, environmental, industrial, medical, and military applications. The WSN consists of a large number of independent, spreading, low-powered devices called sensor nodes that are employed to observe the humidity, position, pressure, sound, temperature, vibration of the surroundings. In WSN, a group of nodes gathers data from the surroundings to achieve particular application purposes [1-3]. Communication among the nodes is done with the help of transceivers. The transceiver of the sensor nodes is normally equipped with omnidirectional antennas. One of the main challenges of WSN is the node size. The node size, as well as the overall sensor size, can be small when the antenna size is small. The smaller the antenna size, the lesser will be power consumption for transception. The design of an appropriate antenna for sensor nodes is a challenging task. Since the antenna occupies the most area of the entire node and it is, therefore, necessary to lessen the antenna size without negotiating its performance. Moreover, to transceive the signal in all directions, the radiation characteristics of the node antenna should be omnidirectional. Microstrip planar antennas have drawn much attention due to their low profile, lightweight, ease of mass production. They are simple and inexpensive to manufacture using currently available PCB technology.

Typically, the frequencies used for WSN include 315 MHz, 433 MHz, 868 MHz, 915 MHz, and 2.45 GHz. The 2.45 GHz industrial scientific medical (ISM) band offers application affability due to the accessibility of large numbers of commercially available RF devices in this band. As the ISM antenna operates with the other narrowband wireless standards such as IMT band (2.3 - 2.4 GHz), WiFi (2.412 - 2.4835 GHz), Zigbee (2.4 GHz), Bluetooth (2.402 - 2.48 GHz), WiMAX (2.30 - 2.40 GHz and 2.496 - 2.69 GHz) and WLAN (2.4 - 2.483 GHz), a wideband antenna that can cover all these narrowband services is therefore necessary. Different antennas have been studied for 2.45 GHz band applications [4-16]. For example, in [5], a textile PIFA antenna was presented for ISM band applications. By introducing slots both in the radiator and ground plane, the designed antenna attained dual operating bands centered at 433 MHz and 2.4 GHz. However, the design has a large size of 140 × 80 mm^2. The antenna presented in [6] is comprised of a patch at the top layer, a ground plane with a slot in the middle layer, and a feedline at the bottom layer and can work at 2.42 - 2.48 GHz band. However, it possesses a large dimension of 100 × 100 mm^2. In [7], a Durer pentagon-shaped antenna was presented for cellular communication and Bluetooth/ RFID applications. With an overall size of 102 × 83 mm^2, the designed antenna achieved a working band ranging from 2.433 to 2.449 GHz. For 2.45 GHz RFID application, in

[9], a circularly polarized antenna was reported that uses a set of slits and slots. However, the antenna is prototyped on an FR4 substrate of dimension 100 × 70 mm^2. For microwave power transmission, in [10], a wideband slot antenna was presented. With an overall size of 80 × 70 mm^2, the studied antenna can work over the 2.16 to 2.88 GHz band. In [11], an antenna was presented to operate in the 2.45 GHz ISM band. The studied antenna is prototyped on the FR4 substrate and the beam switching was achieved by the four-pin diodes. However, it occupies a large area of 80 × 60 mm^2. In [12], a PIFA antenna was reported for ISM applications. Using a shorting pin and a curved slot, the designed antenna attained a bandwidth of 2.39 - 2.55 GHz. However, this design is implanted on a test board of 100 × 40 mm^2. In [13], a planar antenna was reported to operate at dual operating bands. To resonate at 2.4 GHz, it uses a microstrip line while the higher resonance at 3.5 GHz is achieved by the use of two vias. In [14], a modified PIFA was studied to operate at 2.3 GHz. However, the antenna has a 3D structure with a volumetric size of 30 × 28 × 4 mm^3 and is not suitable for portable communications devices. In [15], a simple broadband microstrip patch antenna was presented. It is comprised of a four-sided radiating element and a ground and can operate at 2.4 GHz. However, it occupies an area of 118.23 × 134.04 mm^2 in the Styrofoam dielectric substrate. For ISM band application, in [16], a Z-shaped loop antenna was proposed. The presented antenna is bounded by eight unit cells and is prototyped to work at 2.45 GHz. However, the radius of the presented design is 45 mm and it requires a complex switching structure to achieve reconfigurability. Despite the attainment of the 2.45 GHz band, many of the above-mentioned antennas have the disadvantages of a complex structure, larger dimension, 3D profile. Moreover, some of them operate over two or more frequency bands, which may create unnecessary interference with neighboring narrowband services.

For the 2.45 GHz wireless sensor node application, in this paper, a microstrip planar antenna is presented. The antenna is made up of a rotated A-shaped patch and a small ground plane and is fabricated on the FR4 microwave substrate. To exhibit the resonant mode at around 2.45 GHz, one I-shaped slit is added to the patch and thus the design is enabled to achieve a simulated operating band ranging from 2.3 - 2.6 GHz. The studied design not only has a simple planar structure but also be able to work at around 2.45 GHz narrow-band and can minimize the interference with neighboring wireless services.

2. Antenna design and optimization

The layout of the studied antenna is displayed in Fig. 1. It is made up of a rotating A-shaped radiator and a small ground plane. To achieve the desired operating band, one I-shaped parasitic slit has been added at the right top edge of the rotated A-shaped patch. The breadth and length of the parasitic slit are respectively W_1 and L_1. All the arms of the rotated A-shaped patch have the same width of W_2 mm. The defected ground plane has a dimension of (W-W_3) × L_G, where L_G denotes the height of the ground. The breadth and length of the feed line are chosen respectively as W_3 and L_3. The patch and the feed line are etched on one side of a 1.6 mm-thick FR4 substrate material with ε_r= 4.6, tan δ = 0.02 while the small ground is etched on the opposite side.

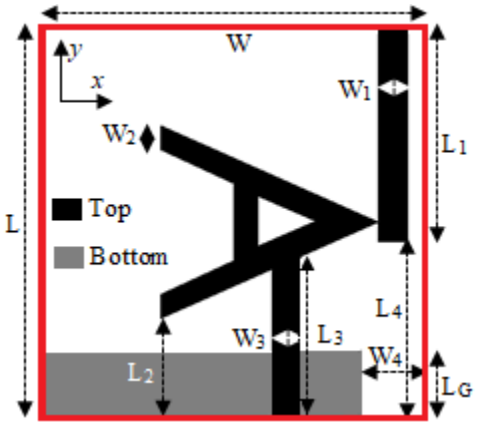

Fig. 1. The layout of the proposed antenna

To transmit the signal, the feedline is connected to a 50Ω SMA connector and a standard SMA model has been considered in simulation to minimize practical SMA interference. The studied A-shaped antenna has an overall size of W × L. The dimensions and parameters of studied antenna are as follows: W_1= 3 mm, L_1= 22 mm, W_2 = 2.5 mm, L_2 = 10 mm, W_3 = 3 mm, L_3 = 16.45 mm, W_4 = 5 mm, L_4 = 18 mm, L_G = 7 mm, W = 40 mm, and L = 40 mm.

To apprehend the design process and working mechanism of the presented antenna, the simulated S_{11} of the different antennas in the evolution process, including Ant 1 (with square patch and small ground plane), Ant 2 (with triangular patch and small ground), Ant 3 (with rotated A-shaped patch and ground) and the proposed one are displayed in Fig. 3 and the steps of the evolution process are shown in Fig. 2. It is clear to see from Fig. 3 that the impedance matching with Ant 1, Ant 2, and Ant 3 for the desired frequency band is very poor. None of these designs can achieve any -10dB operating bandwidth. To achieve the required working band, an I-shaped parasitic slit is added to the Ant 3 to form the anticipated antenna as shown in Fig. 2. The desired working band of the studied antenna is obtained by the fundamental resonant mode of the vertical parasitic slit which resonates at around 2.49 GHz as shown in Fig. 3.

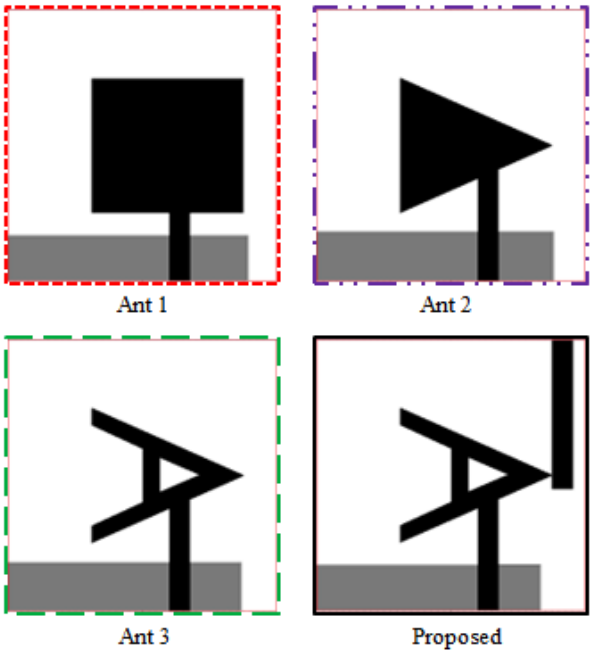

Fig. 2. The design evolution of the proposed antenna (color online)

To clearly understand the working mode, the surface current distribution at 2.45 GHz on the Ant 3(without vertical slit) and the proposed design are shown in Fig. 4. As shown in Fig. 4 (a), the currents are very weak both in the A-shaped patch and the ground plane which indicates a mismatch between them resulting in a poor impedance bandwidth as shown in Fig. 3. On the contrary, in the presented antenna as shown in Fig. 4(b), at around 2.45 GHz the current concentration in the I-shaped slit as well as in the A-shaped patch and feedline is stronger. That is to say, the inclusion of a parasitic slit increases the inductive effect of the studied antenna and enlarges the current path, and hence the slit and the patch form a matching circuit. As shown in the figure, the current concentration at sections ABC and EFG of the radiator is higher than other parts of the antenna. Thus, the resonance at 2.45 GHz is mainly generated by section EFG with the help of section ABC. In section ABC, the current is strong at point A and weak at point C, while in section EFG the current is weak at both points E and G and strong in between them. Therefore, the antenna works at around 0.25-λ mode of section ABC and around 1.5×0.25-λ mode at the section of EFG.

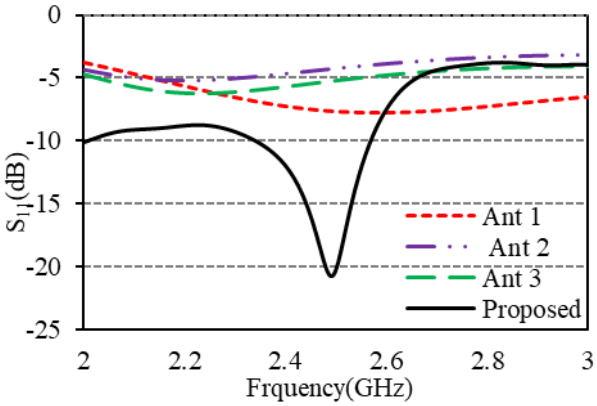

Fig. 3. Simulated S_{11} for different antenna steps (color online)

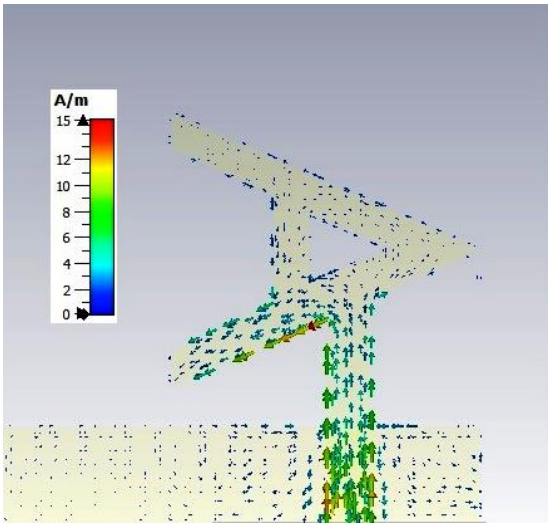

(a)

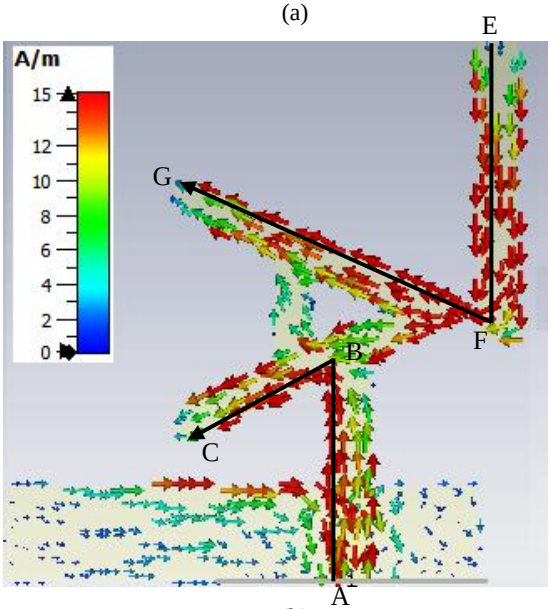

(b)

Fig. 4. Current distribution at around 2.45 GHz (a) on Ant 3 and (b) on the proposed antenna (color online)

The proposed antenna is optimized and simulated using CST microwave studio. The size of all the parameters, including length and width of the parasitic slit, length, and breadth of the feedline, length of the ground plane, and size and position of the rotated A-shaped patch is optimized to get the requisite operating band. Fig. 5(a) shows the variation of S_{11} with feedline breadth, W_3. It is clear to see from the figure that increasing and decreasing the value of W_3 from its optimized value of 3 mm results in a decrement of bandwidth. Moreover, the center frequency moves towards the higher frequency band with W_3. The dependency of impedance bandwidth on ground plane length, L_G is displayed in Fig. 5(b). It is revealed that the longer ground plane can exhibit wider bandwidth with a poor value of S_{11}. In the studied antenna, a length of 7 mm is taken as the final value to realize the required impedance bandwidth with a good S_{11} response.

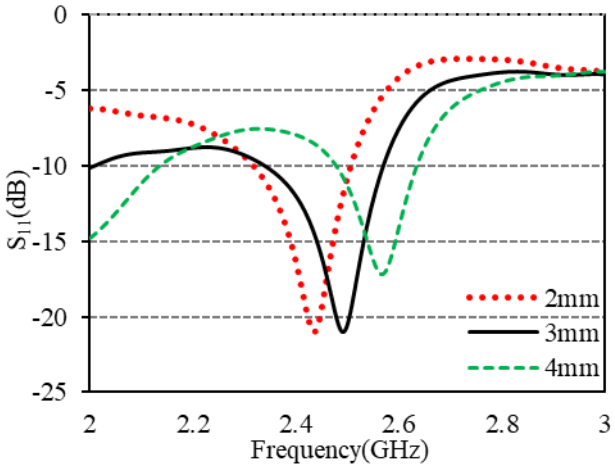

(a)

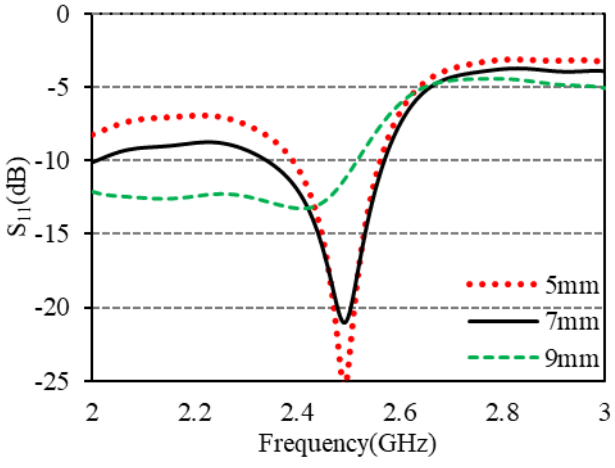

(b)

Fig. 5. Variation of S_{11} for different values of (a) W_3, and (b) L_G (color online)

3. Results and discussion

The optimized design parameters have been found after a comprehensive study of the effect of different structural parameters on antenna performance. A set of the prototype of the anticipated rotated A-shaped antenna has been fabricated for experimental validation and is displayed in Fig. 6. The input impedance characteristics of the studied antenna are measured using the PNA N5227A vector network analyzer. The measured S_{11} is plotted with a simulated one in Fig. 7. For $S_{11} \leq$ -10 dB, the measured impedance bandwidth is 270 MHz (2.30 - 2.57 GHz) and the measured result is very much close to the simulated one. The achieved operating band is wide enough to cover the required bandwidths of 2.4 - 2.5 GHz for the ISM band, 2.3 - 2.4 GHz for the IMT band, 2.402 - 2.48 GHz for Bluetooth, 2.4 GHz for Zigbee, 2.412 - 2.4835 GHz for WiFi, 2.30 - 2.40 GHz and 2.496 - 2.69 GHz for WiMAX, 2.4 - 2.483 GHz for WLAN and 2.484 - 2.491 GHz for Globalstar satellite phone uplink. The slight mismatch between the two results is mainly due to the deficient soldering effects of the SMA connector.

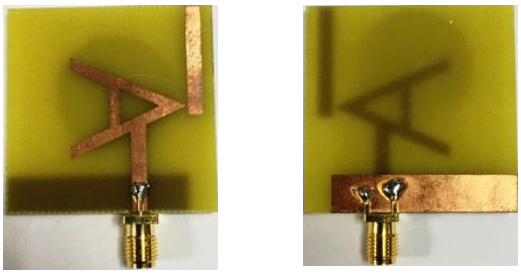

Fig. 6. The prototype of the proposed antenna top view (left) and bottom view (right) (color online)

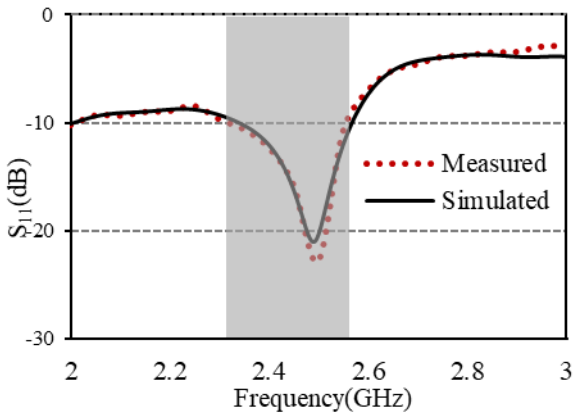

Fig. 7. Measured and simulated S_{11} of the studied antenna (color online)

The radiation characteristics of the fabricated A-shaped planar antenna have been measured using MVG's StarLab near field antenna measurement equipment as

depicted in Fig. 8. The StarLab is capable of measuring the frequency from 650 MHz to 18 GHz. The baseline configuration is obtained by connecting StarLab to a vector network analyzer for passive antenna measurements. The StarLab has the capabilities to measure the gain, efficiency, directivity, beamwidth, radiation patterns, and polarization patterns [17]. Fig. 9 illustrated the measured and simulated peak gain at boresight (positive z) while Fig. 10 shows the radiation efficiency of the fabricated A-shaped antenna. From Fig. 9 it is seen that in the operating band the prototype antenna achieved an average gain of 2.14 dBi with a maximum of 2.40 dBi. The proposed A-shaped antenna also achieved an average radiation efficiency of 83.5 % and the maximum efficiency is 86.4 % as shown in Fig. 10. The lower value of the peak gain of the studied antenna is mainly due to the small effective radiating area. Moreover, it could be due to the high loss of FR4 substrate material that can be improved using a more expensive microwave substrate material rather than standard FR4 material.

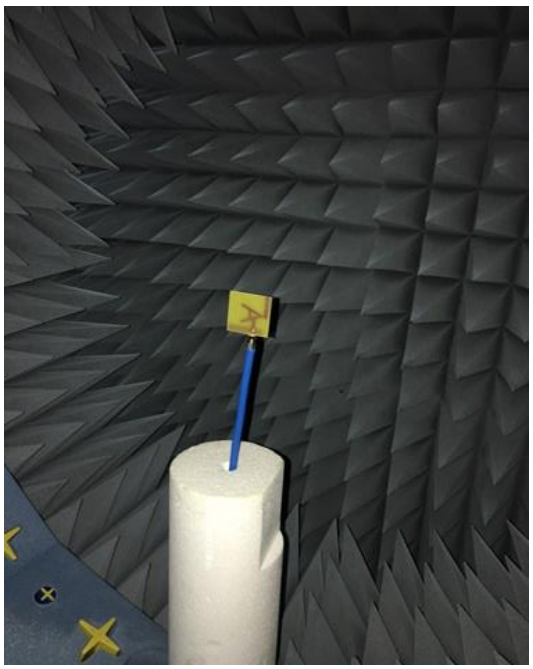

Fig. 8. Radiation characteristic measurement setup in MVG's StarLab (color online)

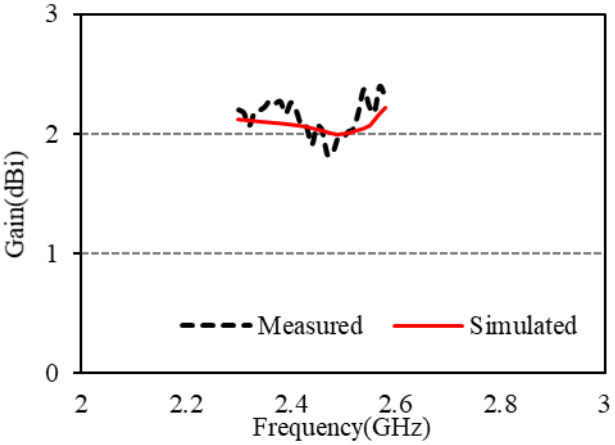

Fig. 9. Measured and simulated peak gain in the operating band (color online)

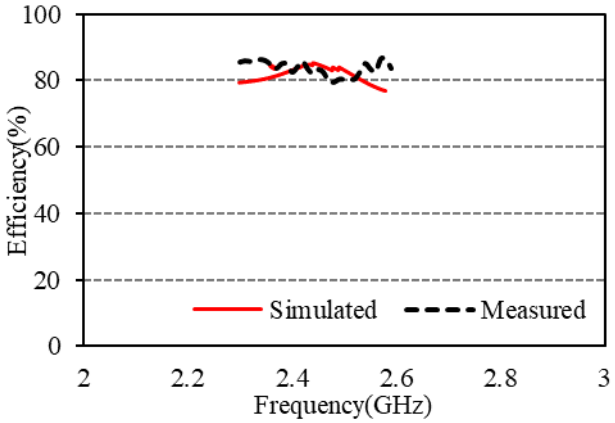

Fig. 10. Simulated and measured efficiency in the operating band (color online)

The measured radiation pattern of the studied antenna at 2.45 GHz is demonstrated in Fig. 11. From the plot, it can be observed that in the *E* (*yz*)-plane the pattern is quite omnidirectional while in the *H* (*xz*)-plane slight deep has been observed in the bore-sight directions. Moreover, in the *H*-plane pattern, a higher cross-polarization component is observed which may be due to the radiation from the non-radiating edges of the proposed asymmetric shape antenna. Moreover, since the studied antenna is fabricated on a microwave substrate with a high dielectric constant, this cross-polarized component becomes significantly prominent near the bore-site direction in the *H*-plane that is reported in [23-28]. Despite the high cross-polarized field in the *H*-plane, from the plot, it can be commented that the radiation patterns of the anticipated antenna are stable and omnidirectional, which is a primary requirement of different narrow-band wireless communication services.

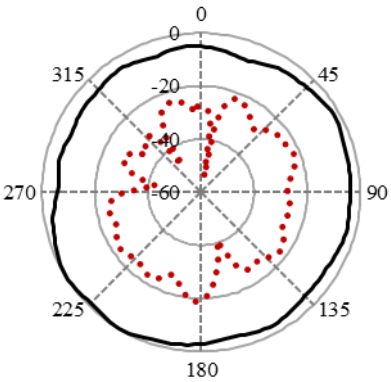

E-plane

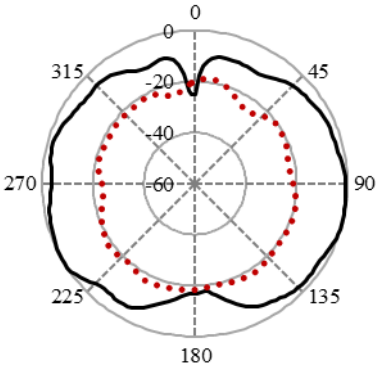

H-plane

Fig. 11. Measured radiation patterns at 2.45 GHz. In the plot, the solid black lines represent the co-polarized components (E_θ) while the dotted red lines represent the cross-polarized components (E_ϕ) (color online)

Table 1. Comparison of the performances of some antennas operating at around 2.45 GHz band

Ref.	Total Size (mm)	Operating Band (MHz)	BW (MHz)	Gain (dBi)
[5]	140 × 80	2.273 - 2.582	309	6.1
[6]	100 × 100	2.42 - 2.48	60	8
[7]	102 × 83	2.433 - 2.449	16	NA
[8]	92 × 92	2.44 - 2.54	100	NA
[9]	100 × 70	2.435 - 2.51	70	7
[11]	80 × 60	Centered at 2.45	-	1.9
[12]	100 × 40	2.39 - 2.55	160	≈ 2.7
[18]	50 × 78	2.16 - 2.49	330	< 3
[19]	60 × 60	2.21 - 2.54	330	3.6
[20]	71 × 46	2.3 – 2.6	300	1.44
[21]	53 × 46.7	2.43 - 2.48	50	2.65
[22]	50 × 40	2.44 - 2.49	50	NA
This work	40 × 40	2.3 - 2.57	270	2.4

The performance of the anticipated antenna is compared with the antennas reported for applications at the same operating band and is presented in Table 1. In general, from data, it is revealed that the studied antenna has the smallest size. Although the antennas reported in [5, 18 -20] have wider bandwidth, their sizes are much larger than the studied ones. In summary, the studied antenna surpasses many of the reported designs owing to its small size, simple footprint, planar profile, and sufficient operating band to cover the 2.45 GHz ISM band and existing IMT, Zigbee, Bluetooth, WiFi, WiMAX, and WLAN wireless bands.

4. Conclusions

In this paper, a low-profile microstrip planar antenna is proposed for wireless sensor network applications. It is made up of a rotated A-shaped radiator with a vertical parasitic slit and a defected ground plane and has an overall electrical size of 0.33λ × 0.33λ × 0.012λ. The addition of an I-shaped parasitic slit forms a matching circuit by enlarging the current path and hence the studied design can achieve a measured operating bandwidth of 270 MHz (2.30 - 2.57 GHz). Moreover, it achieved satisfactory gain, efficiency and demonstrates an omnidirectional radiation pattern which makes it suitable for ISM and other narrow-band wireless applications including IMT, Bluetooth, Zigbee, WiFi, WiMAX, and WLAN.

References

[1] D. Kandris, C. Nakas, D. Vomvas, G. Koulouras, Appl Syst Innov. **3**, 1 (2020).
[2] R. George, T. A. J. Mary, IET Commun. **14**, 715 (2020).
[3] M. Chinnasamy, E. F. Sundarsingh, P. Sankaran, International Journal of RF and Microwave Computer-Aided Engineering **30**, 1 (2020).
[4] R. Azim, M. T. Islam, H. Arshad, M. M. Alam, N. Sobahi, A. I. Khan, IEEE Access **9**, 5343 (2021).
[5] Part 18: Industrial, Scientific and Medical Equipment, FCC Rules and Regulations **1**, 877 (2019).
[6] S. Yan, V. Volskiy, G. A. E. Vandenbosch, IEEE Antennas Wirel. Propag. Lett. **16**, 2436 (2017).
[7] J.-H. Chou, D.-B. Lin, K.-L. Weng, H.-J. Li, IEEE Trans. Antennas Propag. **62**, 5242 (2014).
[8] J. Abraham, A. K. K. John, T. Mathew, in Proc. Intl. Conf. Info. Comm. Embed. Syst., Chennai. India **1** (2014).
[9] R. Ashtari, M. Baginski, R. Dean, Microw. Opt. Technol. Lett. **58**, 2508 (2016).
[10] D. L. Nguyen, K. S. Paulson, N. G. Riley, IET Microw. Antennas Propag. **6**, 94 (2012).
[11] W.-W. Li, Z.-Z. Qin, S.-J. Chen, L. Zhang, Q.-H. Liu, Microw. Opt. Technol. Lett. **60**, 1946 (2018).
[12] A. R. Chandran, S. Morris, S. Raman, N. Timmons, J. Morrison, J. Electromagnet. Waves Appl. **31**, 1333 (2017).

[13] H. W. Liu, C. F. Yang, Electron. Lett. **46**, 113 (2010).
[14] J. Malik, A. Patnaik, M. V. Kartikeyan, IEEE Antennas Wirel. Propag. Lett. **14**, 503 (2014).
[15] V. S. Raviteja, V. R. Laakshmi, Microw. Opt. Technol. Lett. **61**, 1841 (2019).
[16] A. B. Mutiara, R. Refianti, Rachmansyah, J. Theor. Appl. Info. Technol. **33**, 184 (2011).
[17] D. K. Janapala, F. S. Caspe, N. Moses, Intl. J. RF Microw. Comput. Aid. Eng. **29**, 1 (2019).
[18] StarLab: Microwave Vision Group. https://www.mvg-world.com/en/products/antenna-measurement/multi-probe-systems/starlab.
[19] Z. Kang, X. Lin, C. Tang, P. Mei, W. Liu, Y. Fan, Intl. J. Microw. Wirel. Technol. **9**, 977 (2016).
[20] W. Li, Y. Wang, B. You, Z. Shi, Q. H. Liu, IEEE Antennas Wirel. Propag. Lett. **17**, 2459 (2018).
[21] K. N. Paracha, S. K. A. Rahim, H. T. Chattha, S. S. Aljaafreh, S. Rehman, Y. C. Lo, Intl. J. Antennas Propag. **2018**, 1 (2018).
[22] S. Shrestha, S. R. Lee, D.-Y. Choi, Intl. J. Antennas Propag. **2014**, 1 (2014).
[23] Y.-S. Chen, C.-W. Chiu, IEEE Trans. Antennas Propag. **65**, 2305 (2017).
[24] P. Bhartia, I. Bahl, R. Garg, A. Ittipiboon, Microstrip Antenna Design Handbook, Massachusetts, USA, Artech House Publishers (2000).
[25] A. K. M. A. H. Siddique, R. Azim, M. T. Islam, Intl. J. Microw. Wirel. Technol. **11**, 711 (2019).
[26] R. Azim, R. Aktar, A. K. M. M. H. Siddique, L. C. Paul, M. T. Islam, J. Optoelectron. Adv. M. **23**, 127 (2021).
[27] R. Azim, K. Dhar, M. M. Alam, M. T. Islam, Optoelectron. Adv. Mat. **14**, 509 (2020).
[28] R. Azim, A. K. M. M. H. Meaze, A. Affandi, M. M. Alam, R. Aktar, M. S. Mia, T. Alam, M. Samsuzzaman, M. T. Islam, Intl. J. Microw. Wirel. Technol. **13**, 486 (2021).

*Corresponding author: rezaulazim@cu.ac.bd